A Comparison of Finite Control Set and Continuous Control Set Model Predictive Control Schemes for Speed Control of Induction Motors

Abdelsalam A. Ahmed, *Member, IEEE*, Byung Kwon Koh, and Young Il Lee, *Senior Member, IEEE*

***Abstract*—This paper presents a comparative study of two predictive speed control schemes for induction machine (IM) in terms of their design and performance. The first control scheme is finite control set-model predictive control (FCS-MPC) with modulation control and the second control scheme is continuous control set-model predictive control (CCS-MPC) with space vector-pulse width modulation. The two schemes adopt the cascaded control approach, which consists of an inner MPC loop for torque control and outer MPC loop for speed control using two individual cost functions. The outer MPC produces the required torque to drive the IM at the reference speed while the reference torque is taken as the input of the inner MPC, which in turn generates control signals for the inverter. The control states of the two MPCs are constrained with the maximum limits of the drive system. The state feedback is achieved with a standard Kalman filter, which estimates the nonmeasured load torque. For a fair comparison, both approaches are applied to the same IM at the same operational circumstances. The control approaches are implemented and validated in an experimental environment using the same sampling frequency on the same test bench (3.7 kW IM drive). The behavior of the control approaches is assessed by applying reference and disturbance steps to the system in different operational modes. Comparison of the predictive schemes leads to the conclusion that the both MPC approaches achieve similar performances. However, the CCS-MPC scheme has a smaller current ripple and is of low computational complexity. The computing duration is not very different for the three tested schemes. CCS-MPC can cope with a less powerful DSP than for FCS.**

***Index Terms*—Continuous control set-model predictive control (CCS-MPC), field weakening control, finite control set MPC, induction motors, Kalman filter (KF) estimator, speed control, torque constraint.**

Manuscript received January 28, 2017; revised June 1, 2017 and August 22, 2017; accepted September 14, 2017. Date of publication October 2, 2017; date of current version April 3, 2018. This work was supported by the National Research Foundation of Korea under Grant NRF-2017M3A6A6052595 and Grant NRF-2015R1D1A1A01060451. Paper no. TII-17-0134. *(Corresponding author: Young Il Lee.)*

A. A. Ahmed is with the Department of Electrical Power and Machines Engineering, Faculty of Engineering, Tanta University, Tanta 31511, Egypt (e-mail: abdelsalam.abdelsalam@f-eng.tanta.edu.eg).

B. K. Koh and Y. I. Lee are with the Department of Electrical and Information Engineering, SeoulTech, Seoul 01811, South Korea (e-mail: bkkohyes@gmail.com; yilee@seoultech.ac.kr).

Color versions of one or more of the figures in this paper are available online at http://ieeexplore.ieee.org.

Digital Object Identifier 10.1109/TII.2017.2758393

I. Introduction

THE model predictive control (MPC) has been successfully used in industrial applications [1], [2]. In the last decade, the MPC is mostly used for current and torque control of induction machine (IM), and the linear PI controller is used in the outer loop for tracking the speed reference [5]–[7], in which the gains of the PI controllers have to be modified at each operational circumstance.

A cascaded predictive control approach, which regulates the stator currents and speed of the machine individually via two separate cost functions, has been presented in [4] and [8]–[10]. In [4], the torque reference constraint was considered offline. In [9], two cost functions with two different weighting matrices are used in MPC design, which increases the computational burden. Moreover, high ripples are embedded in the current and torque waves. A theoretical implementation for reference speed tracking was presented in [10]. But, the performance of this control method has not been validated by experiment.

Two main groups of predictive control that have been applied in drive applications are deadbeat predictive control [11]–[13] and finite control set-MPC (FCS-MPC) [2], [14]–[16]. The FCS-MPC depends on determination of the optimal voltage vector that minimizes the predefined cost index. This MPC method yields a good transient performance. However, this method causes high ripples in torque and current waves. Research efforts have been conducted on minimizing of torque and current ripples in FCS-MPC by optimizing the time interval in which the selected voltage vector is applied to the inverter [17], [18]. A continuous control set MPC (CCS-MPC) that combines the merits of the deadbeat MPC and FCS-MPC techniques has been applied for torque control of permanent magnet synchronous motor (PMSM) [19]–[21] and of IM [22]. The CCS-MPC is based on voltage calculation via minimization of the cost function for reference tracking.

A comparative study of different predictive current control schemes for PMSMs is performed [20]–[22]. In [20], the performance of FCS and CCS controllers is compared. It showed that both approaches achieve similar performance. The used FCS-MPC is the conventional one, i.e., without modulation control, in which the switching frequency is varied according to the load and speed conditions, whereas the CCS-MPC has a fixed switching frequency. Furthermore, the comparison is implemented in simulation results for a PMSM. In [22], two predictive

control methodologies, i.e., forced machine current control and model predictive direct torque/current control, were presented and compared for IM drives. However, the performance of these methods was evaluated by only simulations for current control. However, from the literature, insufficient research activities have been conducted on FCS-MPC, CCS-MPC, and comparison of their performance for IM drives in a wide-speed range based on direct MPC for speed control; especially when flux control techniques, i.e., flux-increased control (FIC), flux-limited control (FLC), and flux-weakening control (FWC) are all together considered.

The major issue of speed control of electric drives using MPC is the need of estimation of the mechanical load torque that is applied to the controlled machine. The use of Kalman filter (KF) allows the estimation of the measured and nonmeasured variables [10], [23], [24]. In [10], the rotor speed, rotor position, and load torque are observed in a cascaded predictive speed control. The performance of this approach was successfully tested, but only through simulation. The KF in [23] is applied without predictive control, whereas in [9], the speed is controlled using a cascaded two MPC controllers; however, the disturbance representing the load torque is assumed to be constant. The estimated load torque in [24] was successfully tested in simulation, but it presented a worse dynamic performance for the estimated load torque in the experiment.

In this paper, two MPC control schemes are proposed for speed control of IM without use of conventional cascaded PI arrangement. Then, an extensive comparison of the performance of the two MPC schemes is presented. This comparison aims at present two strong competitive MPC, i.e., CCS-MPC and FCS-MPC schemes for driving the IM. The two schemes are based on cascaded MPC controllers to generate output control voltage and torque reference in inner and outer loops, respectively. The presented speed control based on FCS-MPC is the extension of [18] for torque control of IM, whereas the outer loop for speed control is designed in this paper. Moreover, the design process of inner and outer loops of speed control system based on CCS-MPC is presented in this paper. The inner loop is designed for torque control of the IM for a given reference torque. The two schemes adopt three operational modes: FIC, FLC, and FWC. In the literature, the CCS-MPC is used for the current control of PMSM [19]. However, insufficient research activities have been conducted on CCS-MPC considering the FIC, FLC, and FWC trajectories all together for control of IM. These schemes are designed under the constraints of rated voltage and current at low and high speeds. The outer loop for speed control is developed based on a separate MPC, which considers the mechanical dynamics of the IM. This loop generates the reference torque that considers the constraints of torque/speed characteristics of IM. The generated torque reference is constrained by the maximum admissible value at each corresponding speed. Moreover, for a certain load torque in the FWC region, the speed reference is limited to the maximum limit of the IM characteristics. All these constraints, in the inner and outer loops, are calculated online. To compensate the external mechanical disturbances, i.e., load torque, a standard KF is developed to estimate load torque using the measured rotor speed. The performance of both schemes is validated by experimental results at different operating points below and above the base speed. In this research, we compare both approaches and point out benefits and drawbacks.

II. Dynamic Model of an Induction Machine

A. Electrical Dynamic Model of IM

The stator and rotor voltage equations of an IM in the synchronous reference frame are presented in [18]. The dynamic equations of IM can be described with state variable, i.e., stator current components and rotor flux components as

$$\dot{x}(t) = A_c(\omega_e(t))\, x(t) + B_c u(t) \tag{1}$$

where $x(t) = [\, i_{dqs}(t)\ \lambda_{dqr}(t)\,]^T$ is the matrix of state variables. The matrices A_c and B_c are

$$A_c(\omega_e(t)) = \begin{bmatrix} -\frac{1}{\alpha}\left(R_s + \beta^2 R_r\right) + j\omega_e & \frac{\beta R_r}{\alpha L_r} + j\frac{\beta}{\alpha}\omega_r \\ \beta R_r & -\frac{R_r}{L_r} + j(\omega_e - \omega_r) \end{bmatrix},$$

$$B_c = \begin{bmatrix} \frac{1}{\alpha} & 0 & 0 & 0 \end{bmatrix}^T$$

where $j = \left[\begin{smallmatrix} 0 & -1 \\ 1 & 0 \end{smallmatrix}\right]$; $R_s, R_r, L_s, L_r, L_m, \omega_e$, and ω_r denote stator resistance, rotor resistance, stator inductance, rotor inductance, mutual inductance, and rotational speeds of the stator current and rotor, respectively. The vector $u(t) = [\, v_{dqs}\ 0\,]^T$ is the input vector, $\alpha = L_s - L_m^2/L_r$ is the stator transient inductance, and $\beta = L_m/L_r$ is the rotor coupling factor. It is worth while noting that the matrix A_c depends on the instantaneous value of mechanical speed ω_r. The discrete state-space model of the IM is described using the Euler method with the sampling period h. The prediction of the stator current and rotor flux at the next sampling instant can be obtained as

$$x[k+1] = Ax[k] + Bu[k].$$

It can be rewritten as

$$\begin{bmatrix} i_s[k+1] \\ \lambda_r[k+1] \end{bmatrix} = A \begin{bmatrix} i_s \\ \lambda_r \end{bmatrix} + B \begin{bmatrix} v_{dqs}[k] \\ 0 \end{bmatrix} \tag{2}$$

where $A = I_{4\times4} + A_c h$ and $B = B_c h$ are state-space matrices and they are defined in [18]. Then, the electromagnetic torque of the IM in terms of the stator current, rotor flux, and number of poles P is given as

$$T_e = \frac{3}{2}\frac{P}{2}\frac{L_m}{L_r}\left(\lambda_{dr} i_{qs} - \lambda_{qr} i_{ds}\right). \tag{3}$$

The control input $u[k]$ is generated by a 2-level voltage source inverter (VSI) using the space vector-pulse width modulation (SV-PWM). Then, it can be considered as a continuous signal constrained as follows [25]:

$$\sqrt{u[k]^T u[k]} = \|u[k]\| \le V_{\mathrm{smax}} \tag{4}$$

where $V_{\mathrm{smax}} = V_{\mathrm{dc}}/\sqrt{3}$, and V_{dc} is the dc-link voltage.

B. Mechanical Dynamic Model of IM

The relationship that links the inner and outer loop is

$$\dot{\omega} = \left(-B\omega_r + pT_e - pT_L\right)/J \tag{5}$$

where ω_r, J, B, T_L, and p are electrical rotational speed, inertia, friction coefficient, load torque, and pole pairs, respectively. This can be discretized with sampling time $T_{\rm sw}$ using Euler approximation to yield the following state-space description:

$$x_m\,[k+1] = A_m x_m\,[k] + B_m u_m\,[k] + E_m d_m\,[k] \tag{6}$$

where $x_m[k] = \omega_r[k]$ is the state variable, $u_m[k] = T_e^*$ is the input control variable, and the disturbance term d_m represents the load torque $T_L[k]$, assumed to be constant where $A_m = 1 - \frac{B\,T_{\rm sw}}{J}$, $B_m = \frac{p\,T_{\rm sw}}{J}$, and $E_m = -\frac{p\,T_{\rm sw}}{J}$. Actually, the developed torque T_e of (3) should be in the place of $u_m[k]$ of (6). Substituting $u_m[k]$ of (6) by T_e of (3) yields a highly nonlinear system dynamics. Hence, for simplicity, we consider $u_m[k]$ as an independent control signal under the assumption that $u_m[k] = T_e^*$, which is called cascaded modeling. This assumption is adopted to design two cascaded MPCs for speed and torque.

III. MPC Schemes for Torque Control

A block diagram of speed control of IM with different MPCs schemes is shown in Fig. 1. It consists of an inner loop for torque control and outer loop for speed control. The inner loop, in turn, is composed into two stages: computation of reference state and MPC for current control. For a given speed, the corresponding reference torque is generated via the speed control loop. This outer loop consists of four stages: First, the load torque is estimated using KF. Second, the speed reference is constrained according to the estimated load torque and the maximum admissible torque of IM drives. Third, the speed reference is modified using an integrator for zero tracking error at steady state. Finally, a separate MPC is used for generating the torque reference for the inner-loop. When FCS-MPC scheme is used, the output of the inner loop is directly applied to the inverter driver as the optimal voltage vector, whereas when the CCS-MPC is used, the control input voltage is applied to the motor via SV-PWM.

A. Computation of the Reference State for Torque Control

In this section, we introduce how to determine a reference state for torque control to guarantee the most efficient operation while following the given torque reference $T_e^*(k)$. In IM, the rotor flux rotates at the synchronized speed ω_e and the rotational angle θ_e changes accordingly. Considering the principle of indirect FOC [18], the electrical reference state $x^*(T_e^*(k))$ can be defined as follows:

$$\begin{aligned} x^*\left(T_e^*, \lambda^*\right) &= \left[\, i_{ds}^*\ i_{qs}^*\ \lambda_{dr}^*\ \lambda_{qr}^*\,\right]^T \\ &= \left[\, \tfrac{\lambda^*}{L_m}\ \tfrac{2}{3}\tfrac{2}{P}\tfrac{L_r}{L_m}\tfrac{T_e^*}{\lambda^*}\ \lambda^*\ 0\,\right]^T. \end{aligned} \tag{7}$$

The rotor flux reference λ^* in (7) could be determined according to operational region, i.e., FIC, FLC, and FWC. Calculation of λ^* has been presented in [18] for the FIC and FLC regions with FCS-MPC for torque control of IM. In this paper, calculation of the flux reference λ^* in the FWC region is briefly introduced as (8). The principle in [26] is used to derive control state:

$$\lambda^*\,(k) = \frac{1}{\sqrt{\tau_r\ \omega_{\rm sl}^*}} \sqrt{\frac{2}{3}\frac{2}{P} L_r\ \ T_e^*\,(k)}. \tag{8}$$

For a given torque reference T_e^*, the flux reference λ^* could be determined when the slip speed is known. The requested slip speed $\omega_{\rm sl}^*$ of IM can be expressed as

$$\omega_{\rm sl}^* = \frac{1}{\tau_r}\frac{i_{qs}^*}{i_{ds}^*}. \tag{9}$$

The current components in (9) are determined considering the voltage and current constraints as

$$\begin{aligned} {i_{ds}}^* &= \sqrt{\frac{\left((V_{s\max} - I_{s\max} * R_s)/\omega_e\right)^2 - \left(\alpha\, I_{s\max}\right)^2}{L_s^2 - \alpha^2}} \\ i_{qs}^* &= \sqrt{I_{s\max}^2 - {i_{ds}}^{*2}} \end{aligned} \tag{10}$$

where $I_{s\max}$ is the maximum stator current determined by the inverter current rating and the machine thermal rating, whereas $V_{s\max} = V_{\rm dc}/\sqrt{3}$, $I_{s\max}$ and $\alpha = L_s - (L_m^2/L_r)$.

B. FCS-MPC Scheme for Torque Control

In this section, the inner loop for torque control is described based on the method proposed in [18]. Hereafter, a brief description of torque control using FCS-MPC is introduced.

1) Definition of Cost Function for Torque Control: This section presents the cost function of the proposed FCS-MPC method for the discrete-time system (2). For this purpose, the one-step ahead predicted error state is defined based on the reference state $x^*(T_e^*,\ \lambda^*)$ of (7) as

$$e\,[k+1|k] = x^*\,(T_e^*,\ \lambda^*) - x\,[k+1|k]$$

where $x[k+1|k]$ is the one-step ahead prediction of the state $x[k+1]$ obtained from the dynamics (2). Now, the cost function for the proposed control system is chosen as

$$J\,(k) = \left(e\,[k+1|k]\right)^T\ W\ e\,[k+1|k] \tag{11}$$

where $W = W^T$ is a 4×4 symmetric positive definite weighting matrix. The matrix W is chosen so that $J(k)$ becomes a monotonically decreasing Lyapunov function for the error dynamics of the system. For guaranteeing the stability of the system, the condition of

$$W - A^T W A > 0 \tag{12}$$

has to be achieved [18]. After applying the Schur complement, (12) is equivalent to the following linear matrix inequality (LMI) as

$$\begin{bmatrix} Q & QA^T\,(\omega_e) \\ A\,(\omega_e)\,Q & Q \end{bmatrix} > 0. \tag{13}$$

Note that the solution of (13) is not unique and we need to define an optimization problem as $\min\limits_{Q} f(Q)$ subject to (13) where $f(Q)$ is a function of Q determined so that $\min\limits_{Q} f(Q)$ can be solved efficiently with the MATLAB LMI toolbox, where

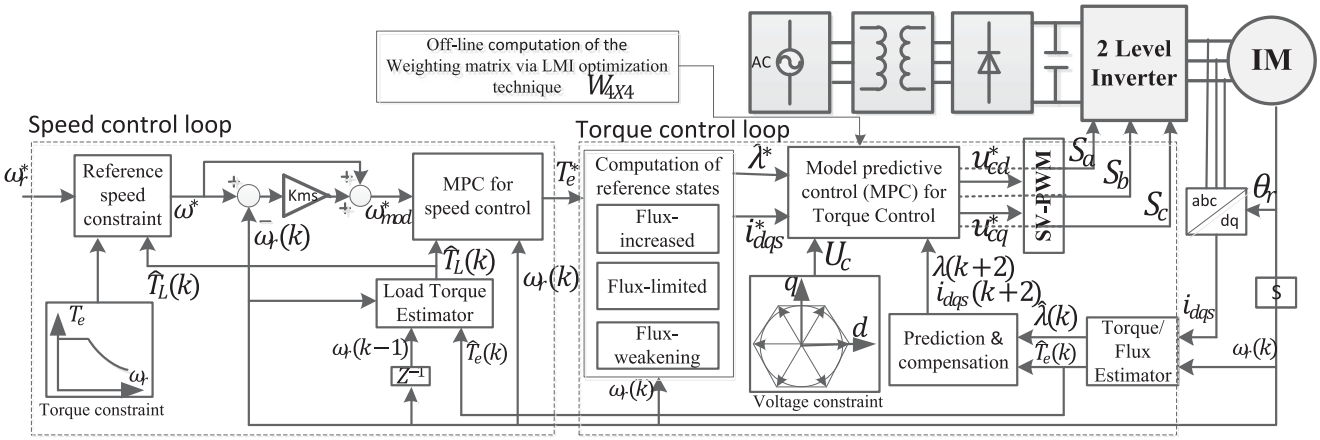

Fig. 1. IM drive employing the inner MPC for torque control and outer MPC for speed control. The SV-PWM module is used in case of CCS-MPC and it is omitted for FCS-MPC.

$Q(= W^{-1})$. The LMI optimization technique is used to find out the value of the weighting factors that achieve the condition of stability. In order to reduce the online computational effort, a set of W is obtained offline depending on the regions of operational speed. For the lack of space, the values of the W matrix at the rated 1500 r/min are given as

$$W = \begin{bmatrix} 2.4 & 0.0 & 75.6 & -49.2 \\ 0.0 & 2.4 & 49.2 & 75.6 \\ 75.6 & 49.2 & 9997.1 & 0.0 \\ -49.2 & 75.6 & 0.0 & 9997.1 \end{bmatrix} * 10^{-4}. \quad (14)$$

2) Design of an FCS-MPC With Optimal Duration: This MPC strategy comprises two steps: find the optimal output voltage vector (v_{sel}) from the eight voltage vectors that yields the smallest cost index $J(k)$ of (11) and computes how long that output voltage vector v_{sel} needs to be applied during the sampling period h to minimize the cost index. In order to determine the optimal output voltage vector v_{sel}, the control input $u[k]$ of (2) should be substituted with each active output voltage vector to produce the predicted value as follows. The system described in (2) is rewritten for all possible active voltage set as

$$x_i\,[k+1|k] = A\,x\,[k] + Bv_i \quad (i = 1,\ \ldots,\ 6)\,. \quad (15)$$

Inserting (15) into the cost index of (11) yields

$$J_i\,(k) = (e_i\,[k+1|k])^T\,W\,(e_i\,[k+1|k]) \quad (16)$$

where $e_i[k+1|k] = x^*(T_e^*,\ \lambda^*) - x_i[k+1|k]$ is the state error for $i = 1,\ \ldots,\ 6$. The output voltage vector v_i^* that yields the smallest value of $J_i(k)$ is chosen to be $v_{\text{sel}}(k)$. Applying v_{sel} over the whole sampling period h will produce a high torque ripple; the application time of v_{sel} is needed to be adjusted. The modulation factor μ is used to adjust the application time of v_{sel}. The predicted state with this modulation factor and v_{sel} is given by

$$x_{\text{sel}}\,[k+1|k] = A\,x\,[k] + B\,\mu\,v_{\text{sel}}\,[k]\,. \quad (17)$$

Then, the cost index in (16) is augmented as follows:

$$J_{\text{sel}}\,(k) = e_{\text{sel}}[k+1|k]^T\,We_{\text{sel}}\,[k+1|k] \quad (18)$$

where $e_{\text{sel}}[k+1|k]$ is the predicted state error with the modulation factor μ; and it can be expressed as

$$e_{\text{sel}}\,[k+1|k] = x^*\,(T_e^*,\ \lambda^*) - \ Ax\,[k] - \ B\,\mu\,v_{\text{sel}}\,[k]\,. \quad (19)$$

Note that (19) is a quadratic equation of modulation factor μ. Thus, the optimal value of μ that minimizes (18) can be obtained from $\frac{\delta}{\delta\mu}J_{\text{sel}}(k) = 0$ as

From (20), at the bottom of the page, the optimal modulation factor μ^* is obtained considering both of torque and rotor flux state error. The rotor flux $\{x[k]\}_{3,4}$ of (2) is estimated and compensation of computational time delay is considered. In order to prevent the steady-state tracking error, the state reference (6) is compensated by integrating the tracking error. Therefore, the modulation factor μ^* is modified accordingly to yield [see (21), below].

$$\mu^* = \frac{BWv_{\text{sel}}\left(x^{*T}\,(T_e^*,\ \lambda^*) - \ A^T x^T\,[k]\right) + v_{\text{sel}}^T B^T W\,(x^*\,(T_e^*,\ \lambda^*) - \ Ax\,[k])}{2v_{\text{sel}}^T B^T WBv_{\text{sel}}} \quad (20)$$

$$\mu^* = \frac{BWv_{\text{sel}}\left(x_s^{*T}\,[k] - \ A^T x^T\,[k+1]\right) + v_{\text{sel}}^T B^T W\,(x_s^*\,[k] - \ Ax\,[k+1])}{2v_{\text{sel}}^T B^T WBv_{\text{sel}}} \quad (21)$$

C. Design of a CCS-MPC Scheme for Torque Control

For the given reference state x^*, a state tracking problem can be formulated as

$$\lim_{k\to\infty} x\,(k) = x^*, \quad \text{subject to } (7)\,. \tag{22}$$

This section presents the MPC method for the discrete-time system (2) to solve the state tracking problem of (22) by minimizing a cost index without any use of numerical methods. For this purpose, a one-step ahead predicted error state $e_x[k+1|k]$ can be defined as

$$\begin{aligned} e_x\,[k+1|k] &= x^* - x\,[k+1|k] \\ &= x^* - (A\,x\,[k] + B\,u\,[k])\,. \end{aligned} \tag{23}$$

Using the foregoing error prediction (23) and based on the reference state $x^*(T_e^*,\ \lambda^*)$ of (7), the cost index for the proposed control system is defined as

$$\begin{aligned} J\,(k) &= (x^*\,(T_e^*,\ \lambda^*) - x\,[k+1|k])^T W\,(x^*\,(T_e^*,\ \lambda^*) \\ &\quad - x\,[k+1|k])\,. \end{aligned} \tag{24}$$

W is a positive definite weighting matrix and $x[k+1|k]$ is the prediction of $x[k+1]$ based on the available data at time k. Note that this cost penalizes the predicted state error at the next time step.

We now consider the input constrained optimization problem associated with $J(x(k), u(k))$

$$\min_{u(k)} J\,(x\,(k), u\,(k)) \quad \text{Subject to } (2) \text{ and } (4). \tag{25}$$

The control $u(k)$ in (2) and (23) is supposed to be applied to the inverter at time step k to minimize the cost index $J(k)$ (24) concerning the predicted state tracking errors at time $(k+1)$. In real applications, however, there is a time delay due to the computation time and modulation mechanism, i.e., the control input computed at time step k is actually applied to the inverter at time step $(k+1)$. This time delay may degrade the performance, and we need to compensate for it. From (2), the prediction $x[k+2|k]$ can be made as

$$x\,[k+2|k] = Ax\,[k+1|k] + Bu\,[k]\,. \tag{26}$$

Based on observation of (26), the cost index (24) is modified as follows:

$$\begin{aligned} J\,(k) &= (x^*\,(T_e^*,\ \lambda^*) - x\,[k+2|k])^T W\,(x^*\,(T_e^*,\ \lambda^*) \\ &\quad - x\,[k+2|k])\,. \end{aligned} \tag{27}$$

The reference states derived in (7) may not be correct because of uncertainties, which lead to a steady-state tracking error. In order to prevent the steady-state tracking error, these state references are compensated by integrating the tracking error:

$$x_s^*\,[k] = x^*\,(T_e^*,\ \lambda^*) + K_s e_s\,[k] \tag{28}$$

where tracking error $e_s[k] = e_s[k-1] + (x^*(T_e^*,\ \lambda^*) - x[k])$ with a proper gain K_s. This compensated reference state $x_s^*[k]$ substitutes for reference state of the cost index (27) to yield

$$J\,(k) = (x_s^*\,[k] - x\,[k+2|k])^T W\,(x_s^*\,[k] - x\,[k+2|k])\,. \tag{29}$$

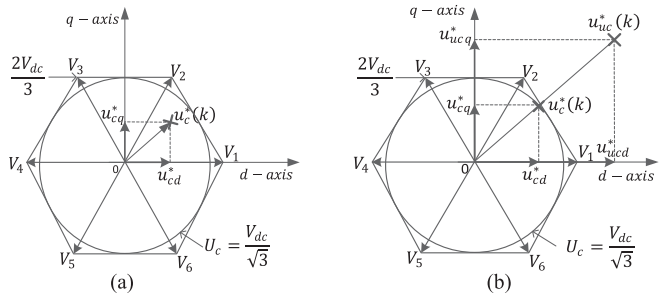

Fig. 2. Input control voltages. (a) Within limits. (b) Unconstrained.

In order to derive the optimizer of the optimization problem (25) explicitly, the cost index (29) is rewritten in terms of the control input $u[k]$ with the help of (26) as

$$\begin{aligned} J\,(k) &= (x_s^*\,[k] - (Ax\,[k+1|k] + Bu\,[k]))^T W\,(x_s^*\,[k] \\ &\quad -(Ax\,[k+1|k] + Bu\,[k]))\,. \end{aligned} \tag{30}$$

Let $u_{\rm uc}^*(k)$ be the unconstrained optimizer of $J(k)$ in (30). Then, $u_{\rm uc}^*(k)$ can be obtained by solving $\frac{\partial J(x(k),u(k))}{\partial u(k)} = 0$ to give

$$u_{\rm uc}^*(k) = \left(B^T W B\right)^{-1}\left(B^T W\,(x_s^*\,(T_e^*,\ \lambda^*) - \mathrm{A}\,x\,[k+1|k])\right). \tag{31}$$

It is apparent that the optimizer $u_c^*(k)$ of the optimization problem in (31) is the same as the unconstraint $u_{\rm uc}^*(k)$ if it is within the limit, i.e., $\|u_{\rm uc}^*(k)\| \le V_{s\max}$, as shown in Fig. 2(a). We now consider the case in which $\|u_{\rm uc}^*(k)\| > V_{s\max}$. Note that the feasible set of inputs satisfying (4) can be represented as a circle in the d-q axis as shown in Fig. 2. Assuming that W is chosen so that $B^T W B = I$ is satisfied, then the level sets of control voltage at all values of the cost function are circles. In this case, it is clear that $u_c^*(k)$ is at the tangential point of the boundary of the circle with the level set of $J(k)$, see Fig. 2(b). Then, the chosen set point of $u_c^*(k)$ is determined by finding the intersection point of the boundary of the feasible input region with the line segment from the point $u(k) = 0$ to $u_{\rm uc}^*(k)$ [19]. Therefore, the MPC algorithm $u_c^*(k)$ is established by

$$u_c^*\,(k) = \begin{cases} u_{\rm uc}^*\,(k) \quad (\text{of } (31)) & \text{if } \|u_c^*\,[k]\| \le V_{s\max} \\ \frac{V_{s\max}}{\|u_c^*\,[k]\|} u_{\rm uc}^*\,(k) & \text{if } \|u_c^*\,[k]\| > V_{s\max} \end{cases}. \tag{32}$$

IV. Constrained MPC for Speed Control

A. Generation of Reference Torque

This section describes the proposed MPC method for the discrete-time system (7). The MPC speed control is designed considering the constraints on control input (32). This speed control loop is used with both the aforementioned two torque control schemes described in Sections III-B and III-C. The torque reference for the inner-loop could be limited with the maximum allowable values according to the ratings of the system. From the torque of (3) with the FOC principles, the

maximum allowable torque could be defined as

$$T^*_{e\_\max} = \begin{cases} \frac{3}{2}\frac{P}{2}\frac{L_m^2}{L_r}\, i^*_{ds}\, i^*_{qs} & \text{when } \omega_r > \omega_{\text{base}} \\ T_{e-\text{rated}} & \text{when } \omega_r \le \omega_{\text{base}} \end{cases} \tag{33}$$

where i^*_{ds} and i^*_{qs} could be found according to different control modes, i.e., FIC, FLC, and FWC. For the purpose of speed control, the cost function of the outer MPC is defined by a quadratic function:

$$J_m = \left(e_m\left[k+1|k\right]\right)^T W_m \left(e_m\left[k+1|k\right]\right) \tag{34}$$

where W_m is the positive definite weighting matrix, which penalizes the tracking offset and control value. Let x^*_m denote the reference speed; the error prediction in speed $e_m[k+1|k]$ is represented as

$$e_m\left[k+1|k\right] = x^*_m - x_m\left[k+1\right]. \tag{35}$$

For zero steady-state error, an embedded integrator is applied to the reference speed. The reference state after integration of $x^*_{\text{ms}}[k]$ becomes

$$x^*_{\text{ms}}\left[k+1\right] = x^*_m + K_{\text{ms}} e_m\left[k+1\right] \tag{36}$$

where K_{ms} is the integrator gain. The predicted error after integrating the error is

$$e_m\left[k+1|k\right] = x^*_{\text{ms}}\left[k+1\right] - x_m\left[k+1|k\right].$$

Applying (7) to (24) by $x^*_{\text{ms}}[k+1]$ yields

$$\begin{aligned} e_m\left[k+1|k\right] = {} & x^*_{\text{ms}}\left[k+1\right] - \left(A_m x_m\left[k\right] + B_m u_m\left[k\right]\right. \\ & \left. + E_m d_m\left[k\right]\right). \end{aligned} \tag{37}$$

Because of the reference state matrix contains only one variable, i.e., the speed ω_r, the value of W_m can be set as 1. Then, the optimal control input T^*_e, minimizing the cost index (34) in each time step, is obtained from $\frac{d}{dT^*_e} J_m = 0$ to give

$$\begin{aligned} T^*_e = {} & \frac{J}{p\, T_{\text{sw}}}\left(e_{\text{ms}}\left[k+1\right] + \frac{B_m\, T_{\text{sw}}}{J} x_m\left[k+1\right]\right. \\ & \left. + \frac{p\, T_{\text{sw}}}{J}\hat{T}_L\left[k\right]\right) \end{aligned} \tag{38}$$

where $e_{\text{ms}}[k+1|k] = x^*_{\text{ms}}[k+1] - x_m[k+1]$ is the speed error, and $\hat{T}_L[k]$ is the estimated value of load torque. The torque of (38) could be considered as the unconstrained optimal control input variable for the inner loop. The produced torque and speed references are constrained considering all possible over load conditions. First, when the IM is commanded to run at a very high speed with a fixed load torque, the reference torque of (38) should be constrained by (33). The reference speed also should be constrained properly when the estimated load torque $\hat{T}_L[k]$ exceeds the maximum admissible torque in FWC region $T^*_{e\_\max}$ of (33). In this case, the reference speed should be reduced to the point so that the maximum admissible torque at that point is equal to $\hat{T}_L[k]$, i.e., the rotor speed that satisfies the condition of (39) is considered as the limited speed reference (40):

$$T^*_{e\_\max}\left(\omega^*_r\right) \le \hat{T}_L\left[k\right] \tag{39}$$

$$\omega^*_r = \omega_r. \tag{40}$$

B. Kalman Filter for Load Torque Estimation

In this paper, the standard KF is applied for estimating the load torque.

1) Model of the Estimator: As depicted in (38), the load torque $\hat{T}_L$ is mandatory to be estimated in order to be properly compensated by the control strategy. The disturbance modeling could be represented as

$$\begin{aligned} \dot{x}_k &= Ax_k + Bu_k + w \\ y_k &= Cx_k + Du_k + v \end{aligned} \tag{41}$$

where $x_k = [\omega_m\ T_L]^T$ is the vector state, $u_k = [T_e]$ is the input, and $y_k = [\omega_m]$ is the measurement. The vector w corresponds to processing noise which stands for the error of the parameters, and v corresponds to measurements noise which stands for the error of the measurement and sample. The state matrices A, B, C, and D are

$$A = \begin{bmatrix} -B/J & -1/J \\ 0 & 0 \end{bmatrix}, B = \begin{bmatrix} 1/J \\ 0 \end{bmatrix}, C = \begin{bmatrix} 1 & 0 \end{bmatrix}, D = [0]. \tag{42}$$

The system (41) in discretization form is

$$\begin{aligned} x_k\left(k+1\right) &= A_d x_k\left(k\right) + B_d u_k\left(k\right) + w \\ y_k\left(k\right) &= C_d x_k\left(k\right) + D_d u_k\left(k\right) + v \end{aligned} \tag{43}$$

where

$$A_d = \begin{bmatrix} \left(1 - \left(BT_{s\omega}/J\right)\right) & \left(-T_{s\omega}/J\right) \\ 0 & 1 \end{bmatrix}, \quad B_d = \begin{bmatrix} \left(T_{s\omega}/J\right) \\ 0 \end{bmatrix}$$

$$C_d = \begin{bmatrix} 1 & 0 \end{bmatrix}, \quad D_d = [0]$$

and $T_{s\omega}$ is the time at which the outer mechanical system is sampled. The time constant of the mechanical subsystem (outer loop) is slower than the electrical subsystem (inner loop). In this case, $T_{s\omega}$ is considered ten times of h.

2) Kalman Filter Implementation: Implementation of KF is processed in two stages. First, the dynamic model of the estimator (43) is used to find out the steady-state values of KF gain for the state variables. This stage is processed offline using MATLAB with speed loop sampling time of $T_{s\omega}$. Then, the process of prediction and correction of the estimated state vector is adopted online. Prediction and correction process is accomplished, respectively, through

$$\hat{x}_{k|k-1} = A_d \cdot \hat{x}_{k-1|k-1} + B_d \cdot u_{k-1} \tag{44}$$

$$\hat{x}_{k|k} = A_d \cdot \hat{x}_{k|k-1} + K_k \cdot \left(y_k - C_d \cdot \hat{x}_{k|k-1}\right). \tag{45}$$

The prediction of state covariance $P_{k|k-1}$ and calculation of KF gain K_k are accomplished, respectively, through

$$P_{k|k-1} = A_d \cdot P_{k-1|k-1} \cdot A_d^T + Q \tag{46}$$

$$K_k = P_{k|k-1} \cdot C_d^T \left[C_d \cdot P_{k|k-1} \cdot C_d^T + R\right]^{-1}. \tag{47}$$

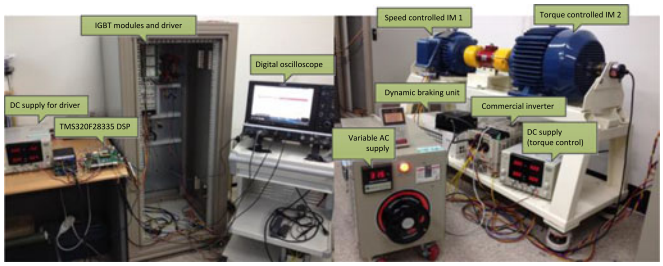

Fig. 3. Photograph of the experimental setup.

TABLE I
INDUCTION MOTOR PARAMETERS

Rated Power [kW]	P_N	3.7
Number of poles	P	4
Rated voltage [V]		220/380
Stator resistance [Ω]	R_s	1.77
Rotor Resistance [Ω]	R_r	1.275
Stator inductance [H]	L_s	0.157
Friction coefficient	B	1e – 5
Power factor		0.875
Rated current [A]		14.2/8.2
Rated speed [r/ min]	ω_N	1740
Rotor inductance [H]	L_r	0.158
Inertia coefficient [kg·m^2]	J	1.5e – 4

In experiment implementation, the noise covariance matrices are defined as follows:

$$Q = \text{cov}\,(w) = E\left\{ww^T\right\} \tag{48}$$

$$R = \text{cov}\,(v) = E\left\{vv^T\right\}. \tag{49}$$

In practice, the matrices Q and R are adjusted by experience because the statistical proprieties of noise cannot be predicted.

V. Experimental Results and Comparison Analysis

A. Experimental Setup

To verify the performance of the two control schemes, an experimental setup has been established as shown in Fig. 3. The setup used for experimental validation consists of a 4-pole, 380 V, 1740/3000 r/min, 3.7 kW IM driven by a laboratory-made 5.6 kW VSI with its interface circuits. The switching devices in the inverters are insulated-gate bipolar transistor (IGBT)s with 20 kHz switching frequency, and dc-link voltage is adjusted at 450 V. The parameters of the motor are presented in Table I. The experimental setup incorporates a control board of TMS320F28335 DSP. The experiments occur at different load torques using 5.5 kW IM driven by a 5.5 kW commercial inverter with vector control in torque control mode. The current was measured directly using a current probe, but the torque and flux responses computed by the embedded controller were transferred to D/A converters and measured by an oscilloscope. The rotor angle is measured using standard incremental encoder with 1024 lines.

In order to reduce the online computational effort, the weighting factors of the cost functions (18) and (30) for FCS-MPC and CCS-MPC methods are optimized offline via the LMI for each

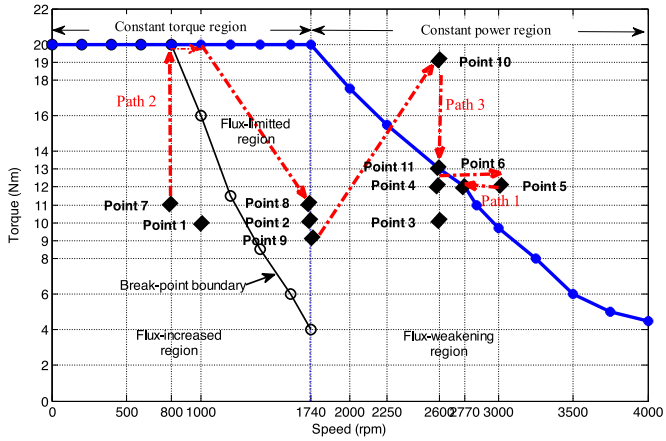

Fig. 4. Experimental results of torque/speed characteristics of IM drive.

accepted speed section. The sampling time of the inner and outer loops is configured by $h = 0.1$ ms and $T_{s\omega} = 1$ ms, respectively. The control method is implemented with sampling frequency of 10 kHz. Computational restriction of the control platform makes the Kalman gain and error covariance matrix is computed offline using KF function in MATLAB.

B. Definition of Operating Points

In this section, the two proposed schemes are validated on the described laboratory test bench. To have a fair comparison, same outer loop for speed control with KF's parameters is followed for both FCS-MPC and CCS-MPC. The dynamic behavior of the controlled IM is tested and validated at different operating points in torque/speed characteristic curve shown in Fig. 4. These points are as follows: point 1 (1000 r/min @ 10 Nm), point 2 (1740 r/min @ 10 Nm), and point 3 (2600 r/min @ 10 Nm), which represent the operation in the areas of FIC, FLC, FWC regions, respectively. Then, torque and speed constraints are tested in three paths to show the operation at torque/speed reference constraints. Path 1 is represented by point 4 (2600 r/min @ 12 Nm), point 5 (3000 r/min @ 12 Nm), and point 6 (2770 r/min @12 Nm) to demonstrate the operation with a constrained reference speed in FWC region. Path 2 is represented by point 7 (800 r/min @ 11 Nm) and point 8 (1740 r/min @ 11 Nm) to depict the performance with constrained reference torque below base speed. Path 3 is represented by point 9 (1740 r/min @ 9 Nm), point 10 (2600 r/min @ 19 Nm), and point 11 (2600 r/min @13 Nm) to test the performance with constrained reference torque above base speed. However, for the sake of page limit, only path 1 will be shown in the following results. The complete experimental results of path 2 and path 3 validate the contribution of this paper. Finally, a thorough comparison between the schemes is presented in terms of their performance characteristics such as speed response, developed torque, estimated load torque, currents, rotor flux linkage, and the torque and speed constraints.

C. Investigation of Dynamic Behavior at Base Speed

Experimental results for a start-up operation followed by a load impact of FCS-MPC and CCS-MPC are shown in

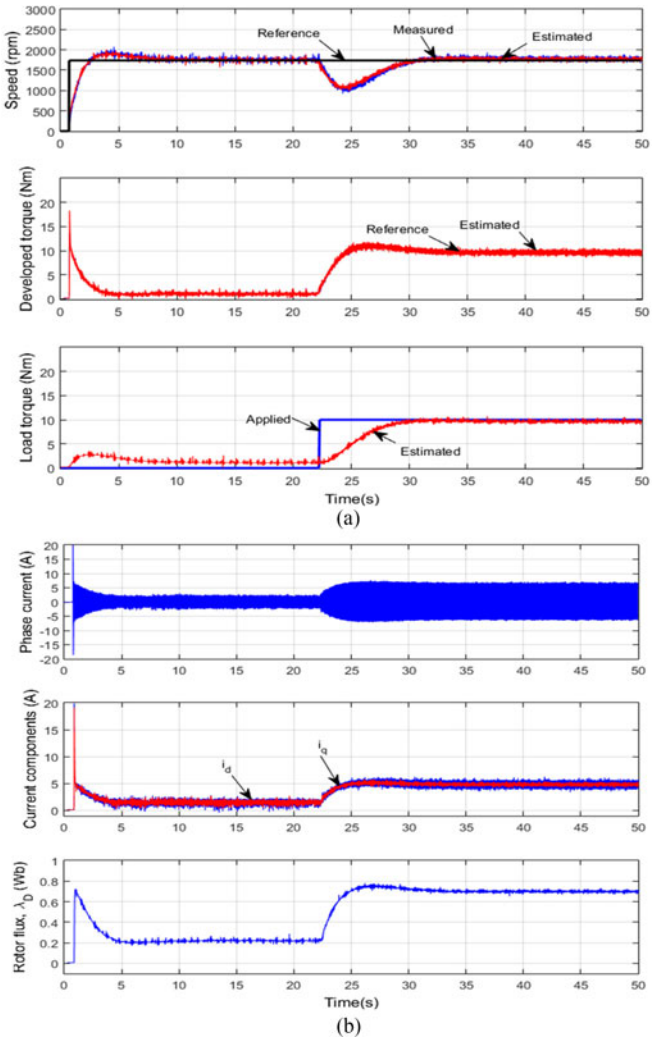

Fig. 5. Experimental results for FCS-MPC: dynamic behavior under step speed from standstill to 1740 r/min and load torque step of 10 Nm: (a) Speed, developed torque, and estimated load torque; and (b) Phase current, i_d and i_q, and rotor flux linkage.

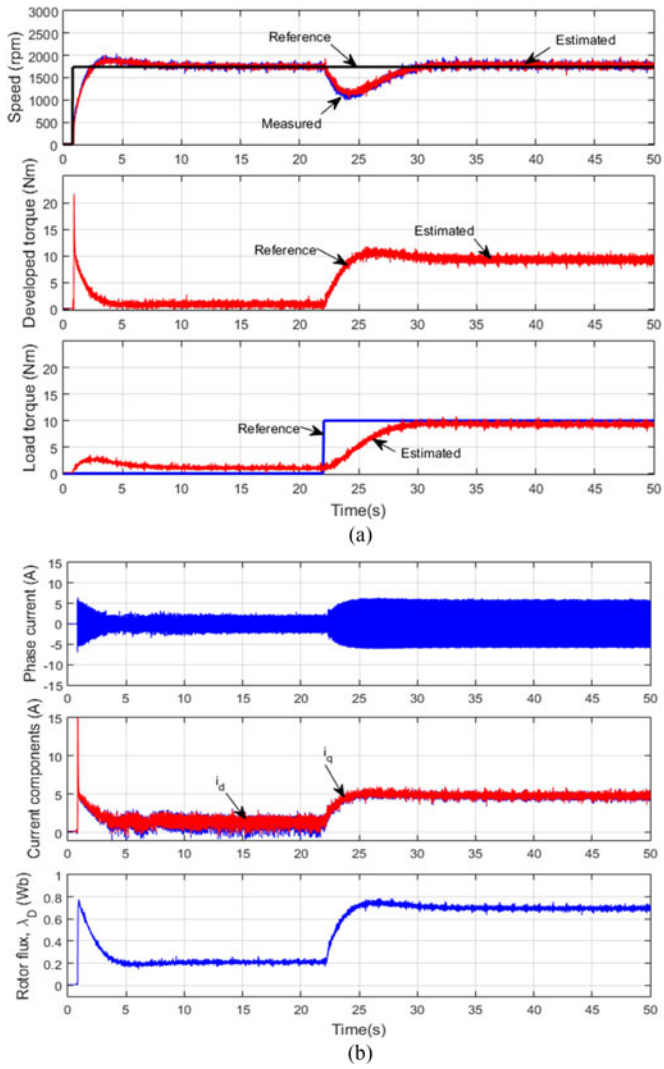

Fig. 6. Experimental results for CCS-MPC: dynamic behavior under step speed from standstill to 1740 r/min and load torque step of 10 Nm: (a) Speed, torques, and estimated load torque; and (b) Phase current, i_d and i_q, and rotor flux.

Figs. 5 and 6, respectively, which adopt FIC and FLC modes. The figures depict the dynamic behavior at startup to rated speed of 1740 r/min. Load torque of 10 Nm is suddenly applied at time of 22 s (point 2 in Fig. 4). As shown in Figs. 5 and 6(a), the rotor speed tracks its reference after 2 s, and good torque response can be noticed from the waves of reference and developed torques. Using very low initial flux of 0.05 Wb causes high overshoot flux-component current which leads to a high initial torque. This case is implemented to test the system at the worst initial condition. However, this phenomenon could be avoided by increasing the initial flux.

A successful implementation of the KF can be noticed by the effective waveforms of estimated load torque and estimated speed. At transient time, the estimated load torque is different from the developed torque because of inertia impact and the difference disappears at steady state. When an external load torque is suddenly applied, some delay in speed response appears. The reason is the delay in KF response to estimate load torque, which strongly affects the reference torque response according to (43). To precisely estimate the load torque with no steady-state error and to save the stator current and the developed torque from high overshot at transient periods, we introduce some delay in response.

Phase current is proportional to the dynamic behavior of IM. At start-up, high current is drawn which depends on the initial flux level and the accuracy of inertia used in the model. Mechanical load torque of 10 Nm is suddenly applied; however, the phase current is gradually increased because of the response of KF estimator. Also, it can be noticed that the rotor flux increases when the load torque is increased (refer to (18) in [18]), and the phase current components are equal in maximum torque per ampere (MTPA) operation [18].

It can be concluded, from Figs. 5 and 6, that the performance of FCS is approximately same as that of CCS. However, the difference lies in that FCS has lower ripples in speed compared to that of CCS. The reason is that the parameters of the outer loop (integrator and KF gains) are specifically designed for

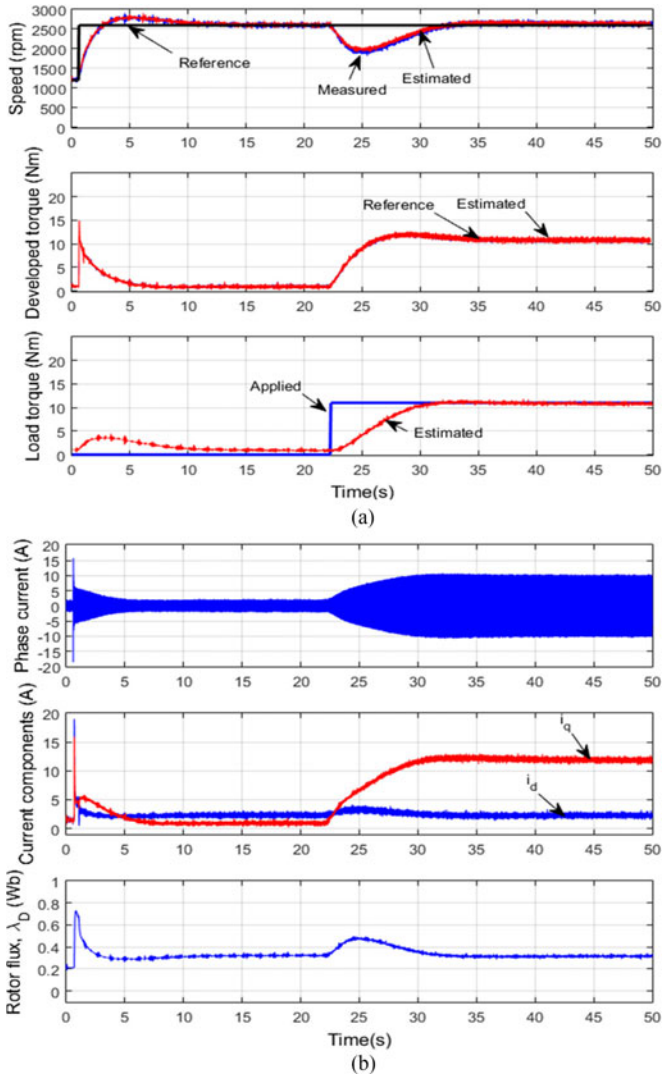

Fig. 7. Experimental results for FCS-MPC: dynamic behavior under step speed from 1200 to 2600 r/min and load torque step of 10 Nm: (a) Speed, torque, and estimated load torque; and (b) Phase current, i_d and i_q, and rotor flux.

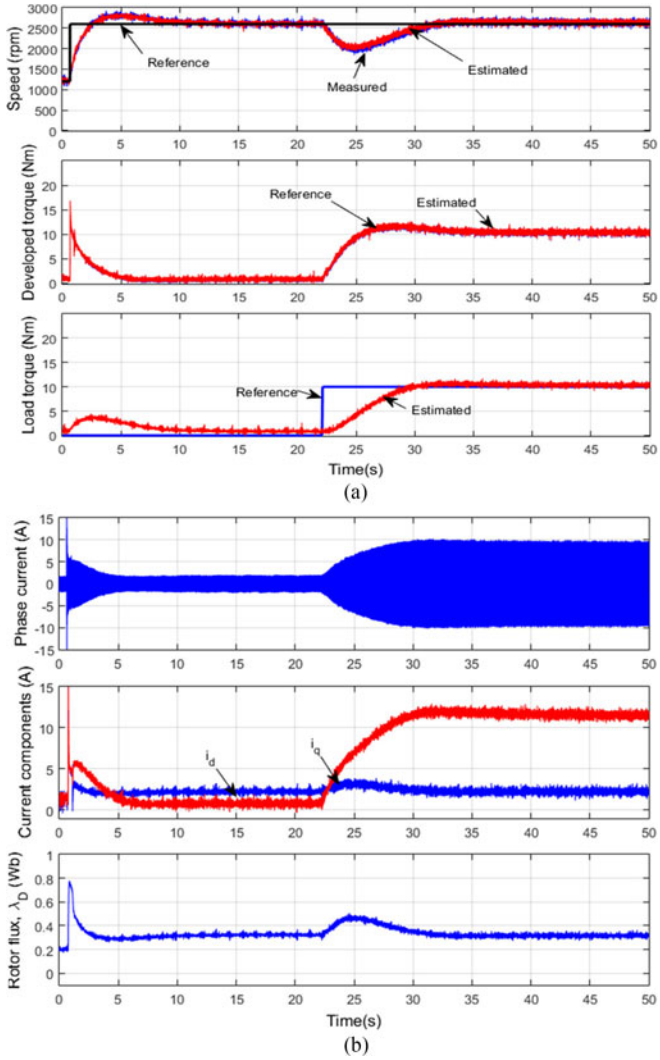

Fig. 8. Experimental result for CCS-MPC: dynamic behavior under step speed from 1200 to 2600 r/min and load torque step of 10 Nm: (a) Speed, torques, and estimated load torque. (b) Phase current, i_d and i_q, and rotor flux.

better performance for FCS, and then they are used for CCS. Therefore, torque reference, generated from the outer loop, with CCS suffers from some ripples.

D. Investigation of Dynamic Behavior Above Base Speed

Experimental results for speed increase followed by a load impact when the IM is driven in FWC region are shown in Figs. 7 and 8 for FCS-MPC and CCS-MPC, respectively. Initially, the IM is run at a steady state of 1200 r/min at no load, and then the reference speed is changed abruptly to 2600 r/min to make the IM drive work in the field weakening operation. Then, an external disturbance that represents load torque is increased abruptly to 10 Nm (point 3 in Fig. 4).

As shown in Figs. 7(a) and 8(a), the applied load torque is precisely compensated by the use of KF estimator with good dynamics (i.e., low-speed drop and approximately null overshot). It can also be noticed in Figs. 7(b) and 8(b) that, with the increase of load torque, the phase current is gradually increased, and the quadrature component of current is increased and it is decoupled to the direct current component. At the transient instants, phase current, rotor flux, and developed torque are drawn within their ratings.

Comparing to the rotor flux in Figs. 5 and 6, it can also be noticed that the rotor flux is weakened when the speed is exceeded above the base value (0.26 Wb $<$ 0.65 Wb at the same load of 10 Nm), which ensures the effectiveness of the FWC. It is also observed from Figs. 7 and 8 that the performance of FCS-MPC is similar to that of CCS-MPC. However, low ripples in speed and torque waves have been noticed with FCS-MPC.

E. Investigation of Constrained Reference Speed in FWC

Here, we would like to demonstrate experimental tests for torque constraint by limiting of speed reference when the

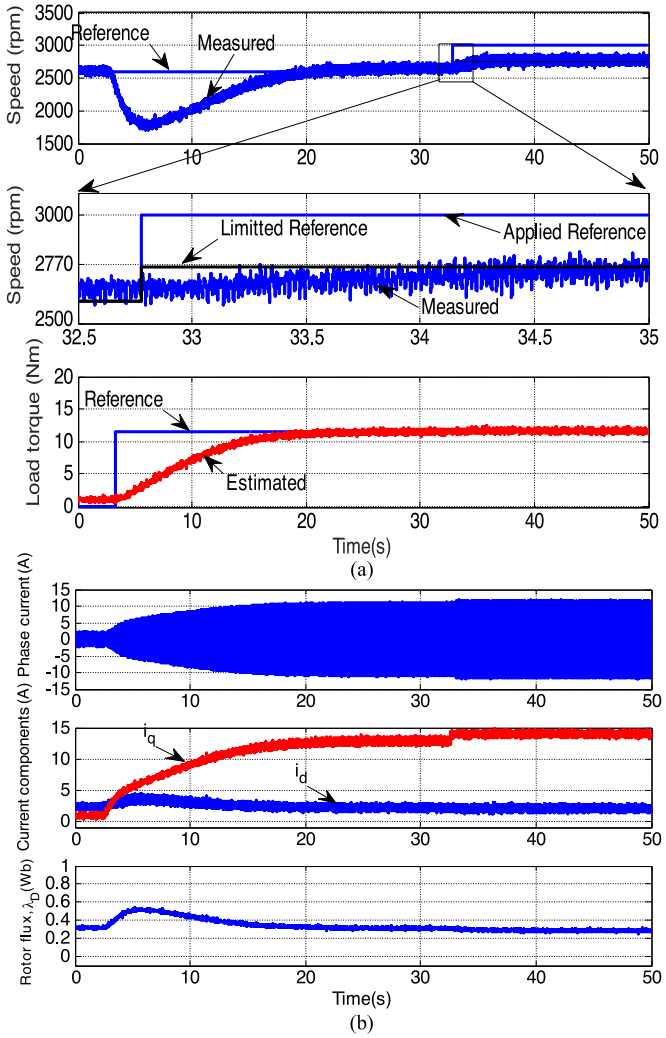

Fig. 9. Experimental results for FCS-MPC: test of constrained reference speed under step change from 2600 to 3000 r/min at 12 Nm: (a) Speed and load torque. (b) Phase current, i_d and i_q, and rotor flux linkage.

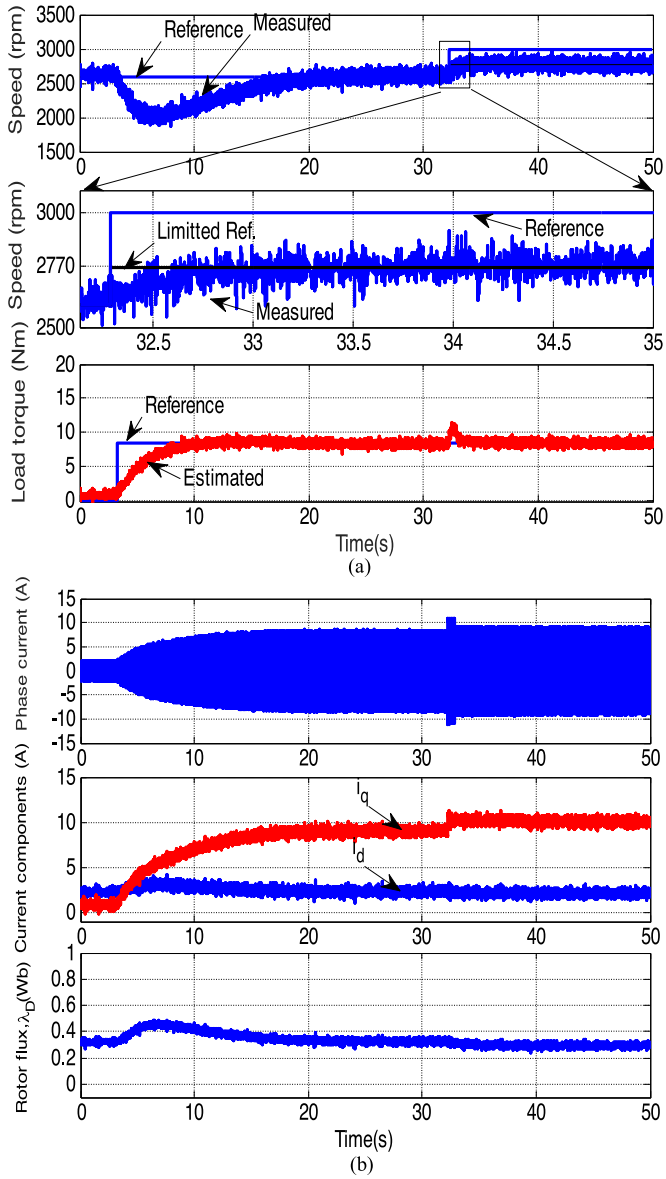

Fig. 10. Experimental results for CCS-MPC: test of constrained reference speed under step change from 2600 to 3000 r/min at 8 Nm: (a) Speed and load torque. (b) Phase current, i_d and i_q, and rotor flux linkage.

operating point transmitted from a point within the boundary (point 4: 2600 r/min @ 12 Nm) to a point exceeds the torque limitation of the IM drive (point 5: 3000 r/min @ 12 Nm), i.e., path 1 in Fig. 4. For FCS-MPC, when we primarily executed that transition at 8 Nm, the speed reached to 3000 r/min and when we executed that transition at 10 Nm, the speed reached to 2850 r/min with high transient period.

For the sake of page limits, only the load torque of 12 Nm is shown to test the speed constraint at FWC as shown in Fig. 9. First, the IM is running at 2600 r/min with a load of 12 Nm (point 4 in Fig. 4), and then speed reference is increased to 3000 r/min. The final destination, i.e., new steady-state operating point, is set above the torque curve limit at 3000 r/min @ 12 Nm (point 5 in Fig. 4). According to the presented technique in Section V using (33), the reference speed and then the measured speed are limited to 2770 r/min at the same load torque of 12 Nm (point 6 in Fig. 4) which is located on the maximum torque curve.

The same tests are performed to CCS-MPC scheme as shown in Fig. 10. The pictures of Figs. 9 and 10 depict a comparison in terms of the constrained speed with maximum admissible load torque for FCS-MPC and CCS-MPC, respectively. As shown in Figs. 9(a) and 10(a), in the enlarged transient period, it can be noticed that the speed reference is increased to 3000 r/min while the limited speed reference reaches to 2770 r/min and the remaining part is ignored. The rotor speed follows the limited reference speed smoothly without any overshot. When the experiment is performed at 12 Nm, high overshoots of speed and torque exceed the maximum limits of the machine. This happens because the parameters of the outer loop are adjusted to the FCS-MPC which, in turn, are used to the CCS-MPC. For a successful operation, the test is performed at 8 Nm with CCS-MPC as shown in Fig. 10. The two figures show that the phase current is slightly increased at the new steady state to produce a reverse flux to weak the rotor flux. The *d*-axis current is slightly

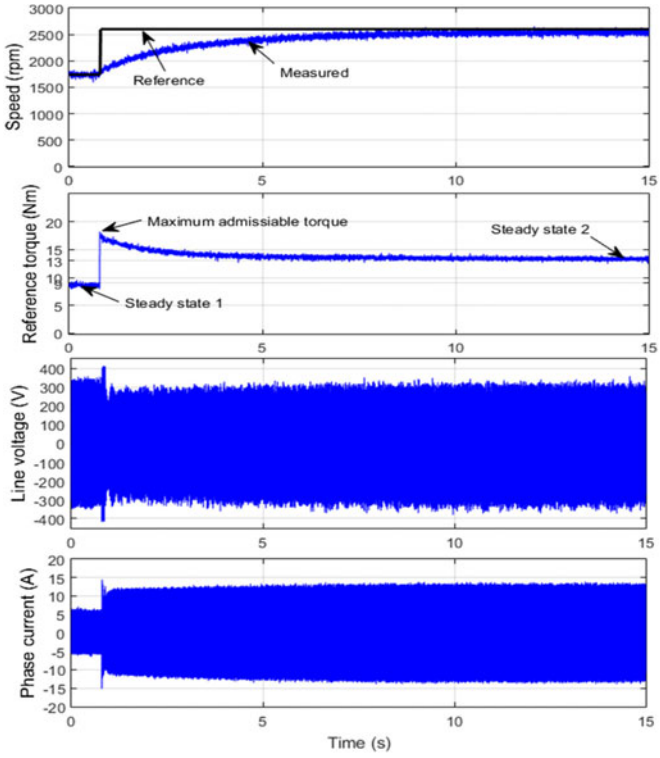

Fig. 11. Experimental results for FCS-MPC: torque constraint in field weakening at 2600 r/min: from top to bottom; reference and measured speeds, reference and measured torques, line voltage, and phase current.

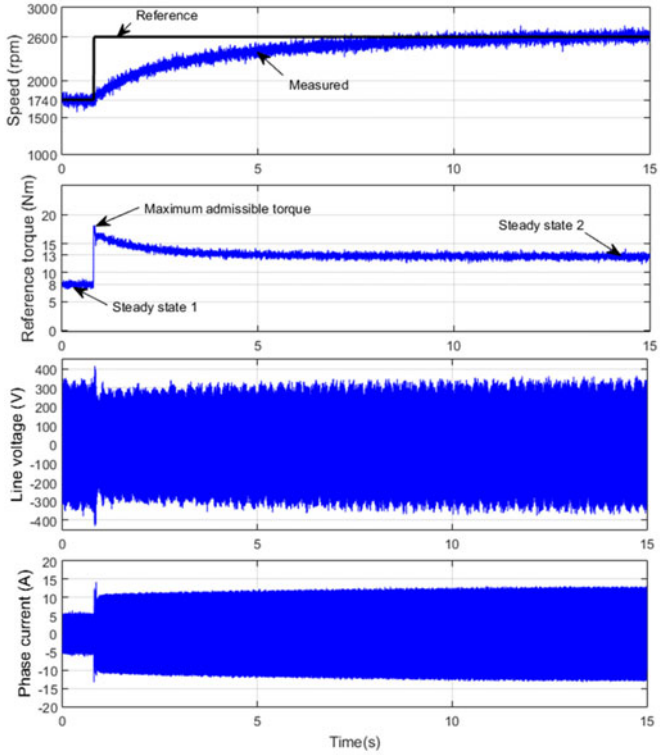

Fig. 12. Experimental results for CCS-MPC: torque constraint in field weakening at 2600 r/min: from top to bottom; reference and measured speeds, reference and measured torques, line voltage, and phase current.

decreased while q-axis component is increased. Also, it can be noticed that the flux in weakened when the speed is increased.

F. Investigation of Constrained Reference Torque in FWC

An experimental test demonstrates the torque constraint at speed acceleration transients by limiting of torque reference. In this case, we scarify by some of acceleration rate. Maximum admissible torque is investigated in FWC region as shown in Figs. 11 and 12 for FCS-MPC and CCS-MPC. First, the IM is run at steady state of 1740 r/min @ 9 Nm (point 9 in Fig. 4). Then, the speed is requested to be increased to 2600 r/min. Thus, the load torque could be increased to 19 Nm (point 10 in Fig. 4). At maximum acceleration instant, it can be seen that the reference torque is increased to 18 Nm, i.e., the maximum admissible torque from (33). Also, at this time, the line voltage is decreased and the phase current is increased. After the transient period is terminated, the line voltage retrieves its steady state, whereas the phase current is raised up to a new steady state (2600 r/min @ 13 Nm), i.e., point 11, Fig. 4.

G. Steady-State Performance

In this section, the steady-state behavior is evaluated. The fast Fourier transform (FFT) analysis and total harmonic distortion of the phase current is shown in Fig. 13(a) for the CCS-MPC and in Fig. 13(b) for the FCS-MPC method. These results are taken when the motor runs at the rated speed of 1740 r/min and is

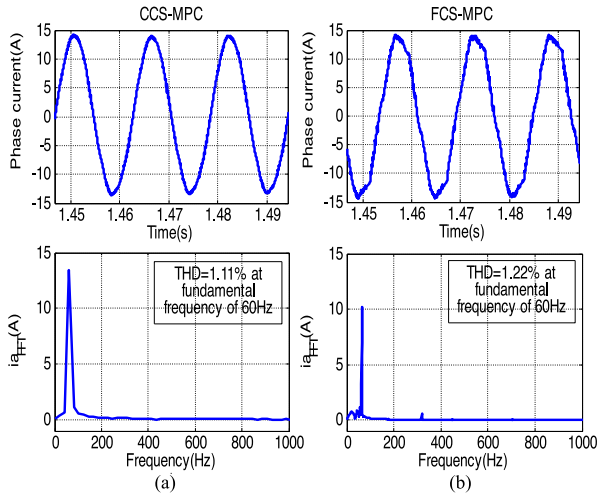

Fig. 13. Simulation results for the phase current and its FFT analysis at the rated conditions (a) CCS-MPC, and (b) FCS-MPC.

loaded at the rated value of 20 Nm. It can be noticed that, for the inner loop, the FCS-MPC method has a little higher harmonic in current wave than that of CCS-MPC.

H. Execution Time

In this section, we compare the computational burden during experimental implementation of the FCS-MPC scheme with and without optimal duration control presented in

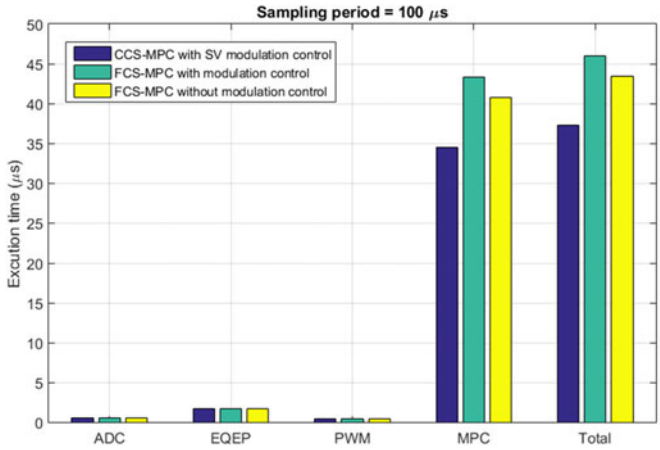

Fig. 14. Computing duration for the tested control schemes.

Section III-B with that of CCS-MPC presented in Section III-C. These durations include the analog-to-digital conversions for currents (ADC), the angular position measure (EQEP), computation of PWM signals which include the comparison between the control signals and the timer's counter, and finally the time of calculation the MPC algorithm. As shown in Fig. 14, it can be found that the time for executing the ADC for the three methods is the same. In addition, the time of EQEP and PWM is the same for the three control methods. However, the time of executing the MPC schemes is different as follows:

1) Time of CCS-MPC includes prediction, reference states, cost function, selection of the optimal voltage vectors, and time for the space-vector modulator.
2) Time of FCS-MPC with modulation control includes prediction, reference states, cost function, selection of the optimal voltage vectors, and time for the modulation control.
3) Time of FCS-MPC without modulation control includes prediction, reference states, cost function, and selection of the optimal voltage vectors.

As seen in the figure, the CCS-MPC provides the lowest computational method, whereas the FCS-MPC with optimal time interval is the highest calculation time consumer.

VI. Conclusion

In this paper, two strong candidates of MPC schemes are presented for speed control of IM. Both FCS with optimal modulation control and CCS are successfully implemented and investigated at different operating conditions with torque and speed constraints. From the experiments, the two control schemes exhibit good dynamic performance keeping all system variables within rated, i.e., rotor flux linkage, stator current, line voltage, and torque. The control systems concern with speed and torque constraints at the worst operational cases with different speed levels and different transient cases. Approximately, same dynamic behavior of IM drive has been obtained by the two MPC schemes. However, torque capability at high-speed levels is increased with FCS compared to that of CCS with little increase in the execution time. Moreover, to get the optimum performance for each, the parameters of the outer loop have to be modified for each MPC scheme separately. With an optimal modulation index for the optimal voltage vector, the FCS could give the same performance of the CCS; however, it costs higher computational burden.

References

[1] A. Linder, R. Kanchan, R. Kennel, and P. Stolze, *Model-Based Predictive Control of Electric Drive*. Göttingen, Germany: Cuvillier Verlag, 2010.
[2] J. Rodriguez and P. Cortes, *Predictive Control of Power Converters and Electrical Drives*. Hoboken, NJ, USA: Wiley, 2012.
[3] E. F. Camacho and C. Bordons, *Model Predictive Control*. New York, NY, USA: Springer, 2013.
[4] Z. Hu and K. Hameyer, "A method of constraint handling for speed-controlled induction machines," *IEEE Trans. Ind. Electron.*, vol. 63, no. 7, pp. 4061–4072, Jul. 2016.
[5] C. A. Rojas, J. Rodriguez, F. Villarroel, J. R. Espinoza, C. A. Silva, and M. Trincado, "Predictive torque and flux control without weighting factors," *IEEE Trans. Ind. Electron.*, vol. 60, no. 2, pp. 681–690, Feb. 2013.
[6] F. Wang, S. Li, X. Mei, W. Xie, J. Rodríguez, and R. M. Kennel, "Model-based predictive direct control strategies for electrical drives: An experimental evaluation of PTC and PCC methods," *IEEE Trans. Ind. Informat.*, vol. 11, no. 3, pp. 671–681, Jun. 2015.
[7] Y. Zhang and H. Yang, "Two-vector-based model predictive torque control without weighting factors for induction motor drives," *IEEE Trans. Power Electron.*, vol. 31, no. 2, pp. 1381–1390, Feb. 2016.
[8] R. Errouissi, M. Ouhrouche, W.-H. Chen, and A. M. Trzynadlowski, "Robust cascaded nonlinear predictive control of a permanent magnet synchronous motor with antiwindup compensator," *IEEE Trans. Ind. Electron.*, vol. 59, no. 8, pp. 3078–3088, Aug. 2012.
[9] S. Chai, L. Wang, and E. Rogers, "A cascade MPC control structure for a PMSM with speed ripple minimization," *IEEE Trans. Ind. Electron.*, vol. 60, no. 8, pp. 2978–2987, Aug. 2013.
[10] C. Garcia, J. Rodriguez, C. Silva, C. Rojas, P. Zanchetta, and H. A. Rub, "Cascaded predictive speed control," in *Proc. 40th Annu. Conf. IEEE Ind. Electron. Soc.*, 2014, pp. 3824–3830.
[11] P. Correa, M. Pacas, and J. Rodriguez, "Predictive torque control for inverter-fed induction machines," *IEEE Trans. Ind. Electron.*, vol. 54, no. 2, pp. 1073–1079, Apr. 2007.
[12] S. A. Davari and D. A. Khaburi, "Sensorless predictive torque control by means of sliding mode observer," in *Proc. IEEE Int. Conf. Power Energy Convers.*, Dec. 2008, pp. 707–711.
[13] S. Alireza Davari, "Predictive direct angle control of induction motor," *IEEE Trans. Ind. Electron.*, vol. 63, no. 8, pp. 5276–5284, Aug. 2016.
[14] A. A. Ahmed, "Experimental Implementation of model predictive control for permanent magnet synchronous motors," in *World Academy of Sci., Eng. Tech.*, vol. 9, no. 7, pp. 679–682, 2015.
[15] A. A. Ahmed, "Fast-speed drives for permanent magnet synchronous motor based on model predictive control," in *Proc. IEEE Veh. Power Propulsion Conf.*, Montreal, 2015, pp. 1–6.
[16] D.-K. Choi and K.-B. Lee, "Dynamic performance improvement of ac/dc converter using model predictive direct power control with finite control set," *IEEE Trans. Ind. Electron.*, vol. 62, no. 2, pp. 757–767, Feb. 2015.
[17] Y. Zhang and H. Yang, "Model predictive torque control of induction motor drives with optimal duty cycle control," *IEEE Trans. Power Electron.*, vol. 29, no. 12, pp. 6593–6603, Dec. 2014.
[18] A. A. Ahmed, B. K. Koh, H. S. Park, K. B. Lee, and Y. I. Lee, "Finite control set model predictive control method for torque control of induction motors using a state tracking cost index," *IEEE Trans. Ind. Electron.*, vol. 64, no. 3, pp. 1916–1928, Mar. 2017.
[19] S. K. Kim, H. S. Park, J. H. Han, and Y. I. Lee, "Stabilizing model predictive control for torque control of permanent magnet synchronous motor," in *Proc. of Chinese Control Conf.*, 2014. pp. 7772–7777.
[20] M. Preindl and S. Bolognani, "Comparison of direct and PWM model predictive control for power electronic and drive systems," in *Proc. IEEE Appl. Power Electron. Conf. Expo.*, 2013, pp. 2526–2533.
[21] F. Morel, X. Lin-Shi, J.-M. Retif, B. Allard, and C. Buttay, "A comparative study of predictive current control schemes for a permanent-magnet synchronous machine drive," *IEEE Trans. Ind. Electron.*, vol. 56, no. 7, pp. 2715–2728, Jul. 2009.
[22] J. Scoltock, T. Geyer, and U. K. Madawala, "A comparison of model predictive control schemes for MV induction motor drives," *IEEE Trans. Ind. Informat.*, vol. 9, no. 2, pp. 909–919, May 2013.

[23] Z. Zedong, L. Yongdong, M. Fadel, and X. Xi, "A rotor speed and load torque observer for PMSM based on extended Kalman filter," in *Proc. IEEE Int. Conf. Ind. Technol.*, 2006, pp. 233–238.
[24] E. J. Fuentes, C. A. Silva, and J. I. Yuz, "Predictive speed control of a two-mass system driven by a permanent magnet synchronous motor," *IEEE Trans. Ind. Electron.*, vol. 59, no. 7, pp. 2840–2848, Jul. 2012.
[25] R. Bojoi, Z. Li, S. A. Odhano, G. Griva, and A. Tenconi, "Unified direct-flux vector control of induction motor drives with maximum torque per ampere operation," in *Proc. IEEE Energy Convers. Congr. Expo.*, 2013, pp. 3888–3895.
[26] J. K. Seok and S. K. Sul, "Optimal flux selection of an induction machine for maximum torque operation in flux-weakening region," *IEEE Trans. Power Electron.*, vol. 14, no. 4, pp. 700–708, Jul. 1999.

Abdelsalam A. Ahmed (M'16) was born in Kafrelsheikh, Egypt. He received the M.S. degree in electrical engineering from Tanta University, Tanta, Egypt, in 2008, and the Ph.D. degree in electrical engineering and automation from Harbin Institute of Technology, Harbin, China, in 2012.

Upon completion of the Ph.D. degree, he was in the Department of Electrical Power and Machines Engineering, Faculty of Engineering, Tanta University, where he is an Assistant Professor. From Jul. 2013 to Jul. 2014, he was a Postdoctoral Fellowship in the Department of Instrumental Science and Technology, School of Electrical Engineering and Automation, Harbin Institute of Technology. From Sep. 2015 to Sep. 2016, he worked as a Postdoctoral Fellowship in the Department of Electrical and Information Engineering, Seoul National University of Science and Technology, Seoul, South Korea. He has authored more than 23 scientific papers in the field of modern strategies of control and drives of electric machines, electric and hybrid electric vehicles, pumping drives, renewable energy sources in microgrids, and power electronics. His current research interests include model predictive control in electrical drive systems and power converters, and electric/hybrid vehicles drive system.

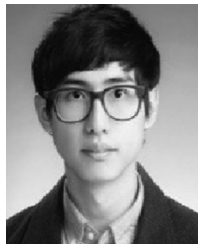

Byung Kwon Koh was born in South Korea, in 1990. He received the B.S. degree in electrical and information engineering in 2015 from Seoul National University of Science and Technology, Seoul, South Korea, where he is currently working toward the M.S. degree in electrical and information engineering.

His research interests include electric machine drives and control engineering.

Young Il Lee (M'99–SM'15) received the B.Sc., M.S., and Ph.D. degrees in control & instrumentation from Seoul National University, Seoul, South Korea, in 1986, 1988, and 1993, respectively.

He worked with Gyeongsang National University from 1994 to 2001 as an Associate Professor, and he has been with Seoul National University of Science and Technology, Seoul, South Korea, since 2001 as a Professor. He visited Oxford University as a Visiting Research Fellow for the period of 1998–1999 and 2007. His research interests include model predictive control and its application to power converters, electrical machines, and electric vehicle.

Dr. Lee served as the Editor of the *International Journal of Control, Automation and Systems*.